Structural and magnetic properties of the Gd-based bulk metallic glasses $GdFe_2$, $GdCo_2$, and $GdNi_2$ from first principles

Raquel Lizárraga
Applied Materials Physics, Department of Materials Science and Engineering, Royal Institute of Technology (KTH), Stockholm SE-10044, Sweden
and Instituto de Ciencias Físicas y Matemáticas, Facultad de Ciencias, Universidad Austral de Chile, Casilla 567, Valdivia, Chile
(Received 18 August 2016; published 1 November 2016)

A structural and magnetic characterization of Gd-based bulk metallic glasses, $GdFe_2$, $GdCo_2$, and $GdNi_2$, was performed. Models for the amorphous structures for two magnetic configurations, ferromagnetic and ferrimagnetic, were obtained by means of a first-principles-based method, the stochastic quenching. In all three cases, the ferrimagnetic configuration was energetically more stable than the ferromagnetic one, in perfect agreement with experiments. In the structural analysis, radial and angle distribution functions as well as calculations of bond lengths and average coordination numbers were included. Structural properties are in good agreement with experiments and do not depend on the magnetic configuration. The distribution of magnetic moments shows that amorphous $GdFe_2$ and $GdCo_2$ are both ferrimagnets, with antiparallel alignment of the magnetic moments of the two magnetic sublattices, whereas Ni nearly loses its magnetic moment in amorphous $GdNi_2$, similar to the situation in its crystalline counterpart.

DOI: 10.1103/PhysRevB.94.174201

I. INTRODUCTION

Bulk metallic glasses (BMG) possess outstanding properties such as high corrosion and wear resistance, high strength and elasticity, and high electrical resistivity. Moreover, due to the lack of grain boundaries they can be shaped into intricate geometries, which make them especially attractive for technological applications [1].

Particularly interesting is the potential application of Gd-based BMGs as refrigerants in magnetic refrigeration technology [2–9]. The magnetocaloric effect (MCE), which is the base of the magnetic cooling cycle, is the thermal response of a magnetic material to the application or removal of a magnetic field. Therefore, materials with large magnetic moments and sizable magnetic entropy changes around the temperature range of interest are considered good candidates for magnetic cooling devices. MCE has been found to be quite large in Gd-based BMGs [3,5], and it has even been shown that the rapid quenching involved in the production of amorphous Gd-transition-metal (TM) alloys significantly increases the low-field MCE [9]. Moreover, because the chemical composition can be varied continuously in glassy alloys, the magnetic ordering temperature can be conveniently tailored [10,11].

Another point to consider when designing a magnetic refrigerant is the refrigeration efficiency, which can be estimated by measuring the refrigeration capacity (RC). This quantity is high if the variation of the magnetic entropy ΔS_m is large for a wide range of temperatures [3]. Very high values of the refrigeration capacity have been reported recently for Gd-based BMGs, $Gd_{53}Al_{24}Co_{20}Zr_3$ and $Gd_{33}Er_{22}Al_{25}Co_{20}$ [5] and $Gd_{55}Co_{20}Al_{25}$ and $Gd_{55}Ni_{20}Al_{20}$ [3], which are much larger than the values found in other well-known crystalline magnetocaloric materials, such as Gd [12] and $Gd_5Si_2Ge_2$ [13]. The observed broadening of the ΔS_m peak in amorphous magnetic materials that gives them their high RC has been attributed to fluctuations of the exchange integral caused by structural disorder [14]. Therefore, understanding the amorphous structure (structural disorder) and its relation to magnetism is crucial for the development of glassy magnetic-cooling materials.

The unique properties of BMG are largely due to their amorphous structure, which forms in the solidification process when the cooling is fast enough to avoid crystallization. However, the absence of a crystal lattice complicates the analysis of experimental data, and therefore, the determination of the amorphous structure can be difficult. This is a drawback to understanding the glassy state and the development of BMGs for commercial applications. Computer simulations can greatly aid the characterization of amorphous materials. Stochastic quenching (SQ) is a technique that can be used with any density functional theory (DFT) method [15,16] to obtain amorphous structures. SQ has proven to be tremendously efficient, fast, and very reliable [17–20].

In this study, the amorphous and magnetic structures of Gd-based BMGs (a-$GdTM_2$, TM = Fe, Co and Ni) were investigated using the SQ method. The a-$GdTM_2$ structures have previously been characterized by means of the anomalous x-ray scattering (AXS) method [21] and x-ray diffraction (XRD) [21–25]. The rare-earth-transition-metal (RE-TM) amorphous systems are a good case study since their magnetic and magnetothermal properties have been extensively investigated [11,21,26–33]. Furthermore, large magnetic entropy changes have been reported in Gd-Co [11,34] and Gd-Ni [35] amorphous ribbons. However, to my knowledge, only a few theoretical investigations have been carried out on a-GdTM alloys [36,37].

II. THEORY

The SQ approach can be used with any first-principles method to produce amorphous structures very efficiently. The SQ procedure for a 150-atom cell is the following: an initial configuration of 150 atoms (100 TM atoms and 50 Gd atoms) is constructed by randomly distributing them in a cubic box with

a constraint that limits the closeness of approach of any pair. This is done in order not to have convergence problems at the beginning of the self-consistent loop. In this case, this distance was set to ∼1.0 Å because Gd is a large atom, but it can be set to much smaller values for smaller atoms. This is an unbiased constraint and has been shown not to affect significantly the final structure [17]. The positions of the atoms in the initial configurations are then relaxed using a first-principles DFT method until the forces on every atom are smaller than 10^{-5} eV/Å. In this way, an amorphous structure is obtained with minimal computational effort. Under the assumptions of the vibrational-transit theory [38] on which the SQ approach is based and provided that the cell size is large enough, this structure is a reliable one because it represents the average amorphous structure of the material under investigation.

In a previous work [18] the authors discussed the cell size effect in the SQ approach, and they determined that a minimum system size of 150 atoms was required to obtain a reliable amorphous structure. Here, two cell sizes were investigated, 150 and 225 atoms. No significant differences were observed between these two cell sizes. Coordination numbers and interatomic distances were almost the same within the expected DFT error. This shows that the 150-atom cell was already large enough to describe the amorphous structures of a-$GdTM_2$ (TM = Fe, Co, and Ni) alloys. The density was chosen to match those in the anomalous x-ray scattering experiment in Ref. [21] (7.85, 8.51, and 8.64 Mg/m^3 for a-$GdFe_2$, a-$GdCo_2$, and a-$GdNi_2$, respectively). These values were estimated from the volume and weight of the samples.

Two ways were devised to handle magnetism when obtaining the amorphous models:

(1) Two separate SQ runs were performed with two different initial spin configurations, ferromagnetic (FM) and ferrimagnetic. The FM configuration had all the atomic spins pointing in the same direction, whereas the ferrimagnetic one had the magnetic moments of Gd and TM atoms antiparallel. In that way atomic positions and spins were relaxed simultaneously.

(2) Once the FM relaxation in method 1 was completed, a new self-consistent cycle was run by keeping the atomic positions fixed, but a ferrimagnetic spin arrangement was assumed. In this way, only the spin configuration was relaxed.

The results show that there is no significant difference between the ferrimagnetic amorphous structures obtained in these two ways regarding all the structural properties studied in this work. Holmström *et al.* showed that for a sufficiently large cell size two amorphous structures relaxed using the SQ approach are statistically indistinguishable [17,18]. They also found that the standard deviation of a Gaussian energy distribution of 1000 amorphous structures (∼150-atom cell) obtained by using the SQ approach is of the order of ∼10 meV [17,18]. This is consistent with the energy difference found between the two ferrimagnetic amorphous structures (8.6 meV/atom for a-$GdFe_2$, 9.3 meV/atom for a-$GdCo_2$, and 5.8 meV/atom for a-$GdNi_2$). For all the cases analyzed here, the two ferrimagnetic amorphous structures produced in the two ways described above are essentially equivalent regarding the atomic structure and the distribution of atomic magnetic moments.

III. COMPUTATIONAL DETAILS

The Vienna ab initio Simulation Package [39,40] (VASP) was used during the quenching together with the local-density approximation with an additional Hubbard U term (LDA+U) [41]. This exchange-correlation functional is well suited to deal with the localized f electrons in rare-earth elements and d electrons in transition metals. Amorphous structures were obtained with the parameter U set to 7 eV for Gd $4f$ electrons and 3 eV for $3d$ electrons for transition metals. These values are in accordance with other *ab initio* calculations on Gd-based amorphous systems in the literature [37] and are standard for RE and TM elements. Tests were performed using $U = 3, 2, 1$ and 0 eV for the transition-metal $3d$ electrons, and there was no observable difference in the amorphous structures; however, the TM magnetic moments were somehow larger than the experimentally observed values for $U = 3,2$, and 1 eV. The eigenstates of the electron wave functions were expanded on a plane-wave basis set using pseudopotentials to describe the electron-ion interactions within the projector augmented-wave approach (PAW) [42].

The convergence criterion for the electronic self-consistent cycle was fixed at 10^{-7} eV per cell, and for the relaxation of the forces on all ions, it was 10^{-5} eV/Å. Calculations were performed at the Γ k point with a cutoff energy of 500 eV. Structural optimizations were performed by using a standard conjugate gradient method during the stochastic quenching procedure.

IV. RESULTS AND DISCUSSIONS

The results presented in this section correspond to the FM amorphous structures for all three glassy materials since there is no appreciable structural difference between the amorphous models acquired assuming FM and ferrimagnetic configurations.

A. Radial distribution functions

The models of the amorphous structures obtained with the SQ method for a-$GdFe_2$, a-$GdCo_2$, and a-$GdNi_2$ were characterized by means of $g(r)$, the radial distribution function (RDF). $g(r)dr$ is the number of atoms between r and $r + dr$ counted from an arbitrary central atom, averaged over all positions of the center atom [43]. In the bottom panels of Figs. 1, 2, and 3 the partial radial distribution functions g_{TM-TM}, g_{Gd-TM}, and g_{Gd-Gd} are shown for the three amorphous systems, respectively. The experimental RDFs obtained by XRD [21] for the three systems are included in the top panels of these figures, respectively.

The position of the minimum after the first peak in the partial RDFs is generally taken as a radial cutoff to determine coordination numbers and bonding distances. The radial cutoffs used in this study are listed in Table I.

In Figs. 1, 2, and 3 the first peak in the total experimental $g(r)$ is split into three contributions. These three subpeaks have been attributed to TM-TM, Gd-TM, and Gd-Gd nearest-neighbor pairs [22,23]. This assumption was confirmed by the AXS [21] experiment where the environmental RDFs around Gd could also be measured. The first peak in the environmental RDF around Gd did not contain any contribution around

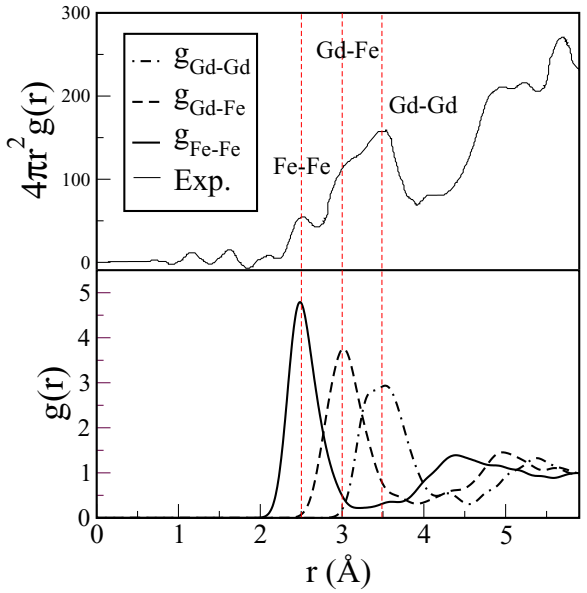

FIG. 1. In the top panel the experimental total RDF obtained by XRD [21] is shown, and the three first-peak positions are indicated by vertical dashed red lines. In the bottom panel, the three calculated partial g_{Fe-Fe} (solid line), g_{Gd-Fe} (dashed line), and g_{Gd-Gd} (dot-dashed line) are displayed.

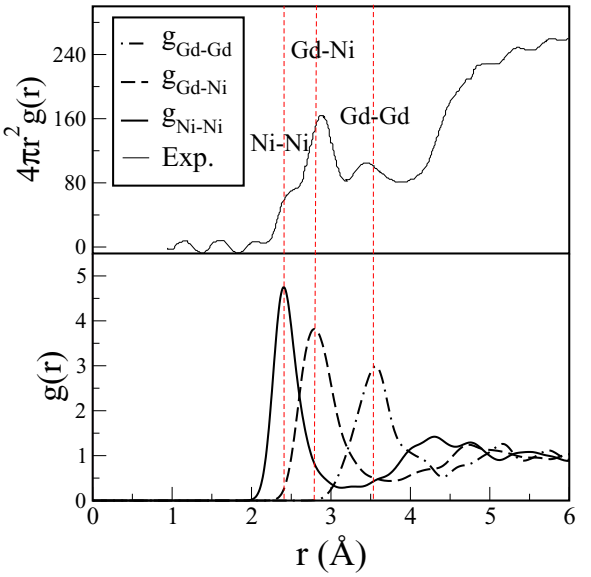

FIG. 3. In the top panel the experimental total RDF obtained by XRD [21] is shown, and the three first-peak positions are indicated by vertical dashed red lines. In the bottom panel, the three calculated partial g_{Ni-Ni} (solid line), g_{Gd-Ni} (dashed line), and g_{Gd-Gd} (dot-dashed) are displayed.

2.50 Å, which is the peak associated with TM-TM pairs. In computer simulations, however, the partial RDFs can be determined individually, and one can clearly see in Figs. 1, 2, and 3 that g_{TM-TM} for all three materials have indeed a main peak located around 2.50 Å.

In experiments, average bonding distances in binary compounds are normally obtained by fitting three Gaussians under the main peak of the total $g(r)$, and the positions of these Gaussians correspond to the average bonding distances. The areas of these three individual Gaussians can be used to determine coordination numbers [22,23]. However, the authors of Ref. [21] used the least-squares variational method [44] to determine structural parameters. Therefore, a comparison of bonding distances becomes less straightforward since it depends on cutoffs and the method used to obtain distances between neighboring atoms. Hence, to avoid confusion, the experimental values given in Table II correspond to the position of the three individual contributions (TM-TM, Gd-TM, and Gd-Gd) of the main peak of the total $g(r)$. The position of the first peak of the calculated partial RDFs and average coordination numbers as determined by SQ are also listed in Table II.

Overall, one can see that the SQ calculations are in excellent agreement with experiments. The largest discrepancies are found for the peak position for TM-TM in a-$GdCo_2$ and the peak position for Gd-TM in a-$GdNi_2$, which are, in both cases, ∼3% smaller than experiments. In Table II one can see that the tendency of the interatomic distances between TM and Gd ions to decrease in the series TM = Fe, Co, and Ni is observed in both amorphous and crystalline counterparts as well as in the SQ structural models.

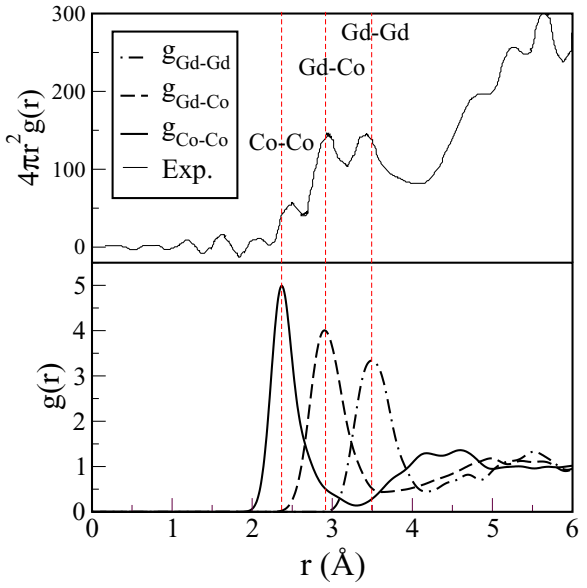

FIG. 2. In the top panel the experimental total RDF obtained by XRD [21] is shown, and the three first-peak positions are indicated by vertical dashed red lines. In the bottom panel, the three calculated partial g_{Co-Co} (solid line), g_{Gd-Co} (dashed line), and g_{Gd-Gd} (dot-dashed line) are displayed.

TABLE I. Radial cutoffs.

	Gd-Gd (Å)	Gd-TM (Å)	TM-TM (Å)
$GdFe_2$	4.52	3.95	3.14
$GdCo_2$	4.16	3.70	3.29
$GdNi_2$	4.36	3.75	3.29

TABLE II. The $g_{\alpha\beta}$ first-peak position and coordination numbers for some selected Gd-TM amorphous alloys.

System	Method	First-peak position (Å)			Average coordination number		
		Gd-Gd	TM-Gd	TM-TM	Gd-Gd	TM-Gd	TM-TM
$GdFe_2$	SQ	3.45	3.09	2.47	6.3	4.8	6.2
$GdFe_2$ (BMG)[a]	AXS/XRD	3.44	3.01	2.48	7.0 ± 0.5	2.5 ± 0.5	6.3 ± 0.5
$GdFe_2$ (BMG)[b]	XRD	3.45	3.05	2.51	6.0 ± 1.0	3.3 ± 0.3	6.3 ± 0.5
$GdFe_2$ (amorphous film)[c]	XRD	3.45	3.00	2.45	6.5		4.5
$Gd_{33}Fe_{67}$ (amorphous ribbons)[d]	XRD	3.45	3.05	2.51	5.3 ± 0.5	3.2 ± 0.5	6.1 ± 0.5
$Gd_{33}Fe_{67}$[e]	DRPH model	3.47	3.01	2.51	6.21	4.03	6.17
$GdFe_2$ (crystal)[b]	XRD	3.18	3.05	2.60	4	6	6
$GdCo_2$	SQ	3.49	2.89	2.36	5.7	4.6	5.9
$GdCo_2$ (BMG)[a]	AXS/XRD	3.40	2.93	2.44	5.8 ± 0.5	3.0 ± 0.5	5.9 ± 0.5
$Gd_{32}Co_{68}$ (amorphous film)[f]	XRD	3.45	2.95	2.50			
$GdCo_2$ (crystal)[a]	XRD	3.14	3.01	2.57	4	6	6
$GdNi_2$	SQ	3.54	2.78	2.40	6.4	4.6	5.8
$GdNi_2$ (BMG)[a]	AXS/XRD	3.49	2.86	2.44	3.5 ± 0.5	4.2 ± 0.5	6.2 ± 0.5
$GdNi_2$ (crystal)[a]	XRD	3.12	2.99	2.55	4	6	6

[a]Experiments taken from Ref. [21].
[b]Experiments taken from Ref. [22].
[c]Experiments taken from Ref. [24].
[d]Experiments taken from Ref. [25].
[e]Experiments taken from Ref. [36].
[f]Experiments taken from Ref. [23].

Coordination numbers were obtained by integrating the corresponding partial RDFs $g_{\alpha\beta}$ up to the radial cutoff,

$$n_{\alpha\beta} = 4\pi\rho_\beta \int_0^{R_{\text{cutoff}}} g_{\alpha\beta}(r) r^2 dr, \tag{1}$$

where α and β are indices over atoms. It can be noted in Table II that the experimentally obtained value for $n_{\text{TM-Gd}}$ increases in the series Fe-Co-Ni; however, the SQ value does not change much. In fact coordination numbers for TM-Gd in a-$GdFe_2$ and a-$GdCo_2$ are much smaller than the corresponding values obtained by SQ but agree well in the case of $GdNi_2$. Interestingly, calculations using a dense random packing of hard spheres (DRPHS) model for the amorphous structure and the local muffin-tin orbital in the atomic sphere approximation (LMTO-ASA) to resolve the electronic structure overestimated the value of $n_{\text{Fe-Gd}}$ as well [36]. Finally, the SQ average coordination number of Gd-Gd neighbors in $GdNi_2$ is larger than the value reported in Ref. [21]. Unfortunately, no other experiments could be found to shed light on this issue. As a matter of fact, the coordination number for Gd-Gd also varies a lot in experiments but not much in SQ. The SQ calculated value of $n_{\text{TM-TM}}$ remains constant for Fe, Co, and Ni, in accordance with experiments.

Crystalline $GdFe_2$, $GdCo_2$, and $GdNi_2$ all have the C15 cubic Laves phase of $MgCu_2$ [45]. The interatomic distances $r_{\text{Gd-Gd}}$, $r_{\text{TM-Gd}}$, and $r_{\text{TM-TM}}$ in crystalline $GdFe_2$ are 3.18, 3.05 and 2.60 Å [22], respectively. They do not differ very much from their amorphous counterparts, except for $r_{\text{Gd-Gd}}$, which is significantly smaller than in a-$GdFe_2$. The same trend is observed in the other two amorphous alloys. Coordination numbers are, however, very different in the Laves structure, $n_{\text{Gd-Gd}} = 4$, $n_{\text{TM-Gd}} = 6$, and $n_{\text{TM-TM}} = 6$.

In summary, by comparing the amorphous and crystalline structures, one can see that Gd atoms gain, on average, two Gd neighbors and the distance between them increases to accommodate the extra atoms in the amorphous compounds, whereas the TM atoms lose, on average, 2 Gd neighbors. The number of TM neighbors around TM atoms and the TM-TM distance are the same in both the amorphous and crystalline alloys.

B. Angle distribution functions

In Fig. 4 the angle distribution functions (ADFs) for all three systems are displayed. The angle distribution functions of crystalline $GdFe_2$, represented by Gaussians to improve readability, are also included for comparison. One can observe no major differences among the three amorphous systems. All six ADFs have similar structures, that is, a high and narrow peak at angles below 100° and a broader peak located between approximately 100° and 120°. The ADFs for Gd-Gd-TM and TM-Gd-TM have the first narrow peak at ∼50°, and those for Gd-TM-Gd have the peak at ∼70°; the rest of the ADFs have the peak at around ∼60°. Comparison with the crystalline ADFs shows that the narrow first peak in the amorphous ADFs is a remnant from the crystalline Laves structure. The broader peak in the amorphous ADFs is, however, formed by the combination of two or three peaks in the crystalline ADFs. In the crystalline ADFs for TM-TM-TM, Gd-TM-Gd, Gd-Gd-TM, and Gd-Gd-Gd there is a peak around ∼180° which is totally absent in the corresponding amorphous ADFs. The Gd-TM-TM ADF also has a peak at ∼30° that is not observed in the corresponding amorphous ADFs.

As one may expect, there is not much difference between the crystalline and amorphous ADFs for TM-TM-TM atoms since the number of TM-TM neighbors and the distance between them do not differ much.

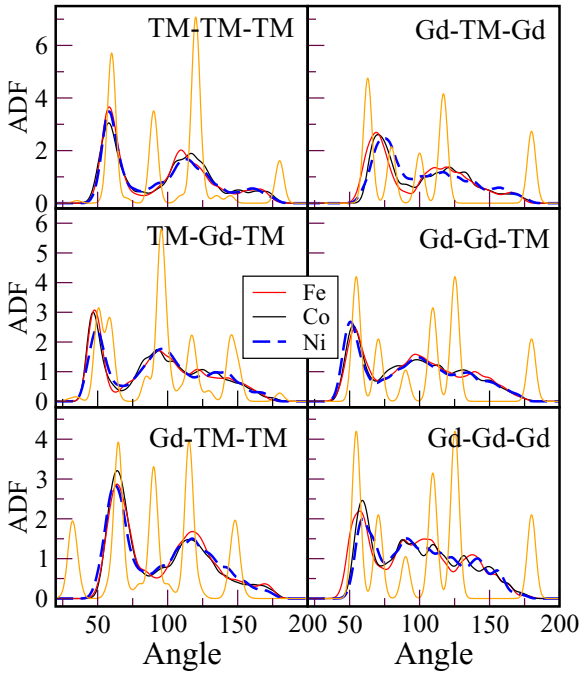

FIG. 4. Angle distribution functions for TM-TM-TM, TM-Gd-TM, Gd-TM-TM, Gd-TM-Gd, Gd-Gd-TM, and Gd-Gd-Gd atoms where TM = Fe (red), Co (black), and Ni (blue). The orange curves correspond to smeared ADFs for crystalline $GdFe_2$.

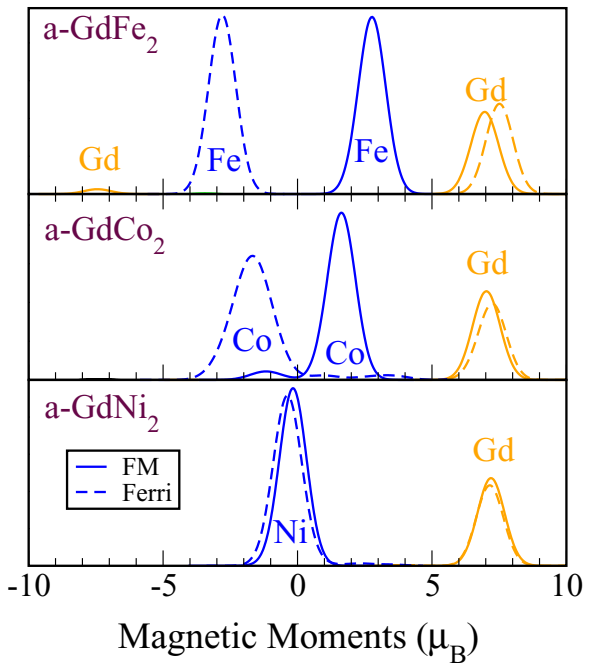

FIG. 5. Magnetic moment distribution for Gd and 3d transition metals for $GdFe_2$ (top panel), $GdCo_2$ (middle panel), and $GdNi_2$ (bottom panel). Solid and dashed lines correspond to the ferromagnetic and ferrimagnetic configurations, respectively.

V. MAGNETISM

Two magnetic configurations were considered in this study, FM and ferrimagnetic. As discussed in the theory section, the ferrimagnetic configuration was produced in two different ways, and these two methods turned out to be equivalent. In the following, the results for the ferrimagnetic structure produced in method 1 and the FM configurations are described.

The ferrimagnetic configuration is energetically favored by $\sim$0.1 eV/atom in a-$GdFe_2$, $\sim$0.07 eV/atom in a-$GdCo_2$, and $\sim$0.008 eV/atom in a-$GdNi_2$. The distributions of magnetic moments of the three systems are shown in Fig. 5. The peaks corresponding to FM and ferrimagnetic configurations are depicted with solid and dashed lines, respectively.

Variation of the U (0–3 eV) parameter for 3d transition metals affected mainly the value of the magnetic moment of the transition metals. For higher values of U, the TM magnetic moments become higher than experiments. In the following, the values of the magnetic moments for $U = 0$ (and 3) eV are reported. In the top panel of Fig. 5, a-$GdFe_2$ in the FM configuration exhibits two peaks associated with Gd, one at $6.91\mu_B$ and the other at $-7.4\mu_B$. There are two other peaks corresponding to Fe, one at $2.25\mu_B$ ($2.7\mu_B$) and the other at $-3.4\mu_B$ (this peak does not show in the present scale). The ferrimagnetic configuration has a Gd peak located close to the FM one at $7.33\mu_B$ ($7.5\mu_B$) and a Fe peak at $-2.4\mu_B$ ($-2.8\mu_B$).

The middle panel of Fig. 5 displays the distribution of the magnetic moments for a-$GdCo_2$. In the FM configuration, one can also observe two peaks associated with Gd, placed at $-7.4\mu_B$ (too small to be seen in the present scale) and $6.94\mu_B$ ($7.02\mu_B$) and two peaks corresponding to Co at $-0.92\mu_B$ ($-1.17\mu_B$) and $1.3\mu_B$ ($1.62\mu_B$), respectively. The ferrimagnetic configuration presents two peaks, one peak at $7.3\mu_B$ ($7.24\mu_B$) corresponding to Gd ions and another peak for Co atoms at $-1.47\mu_B$ ($-1.7\mu_B$).

The bottom panel of Fig. 5 shows the distribution of magnetic moments for a-$GdNi_2$, where only two peaks can be seen for the FM state, one for Gd at $7.2\mu_B$ and the other for Ni at $-0.17\mu_B$. The ferrimagnetic state looks very similar, and the two peaks nearly coincide with the FM ones at $7.12\mu_B$ and $-0.17\mu_B$ ($-0.25\mu_B$), respectively. One can note from Fig. 5 that the magnetic moment of Gd stays almost the same in the three glassy systems, slightly higher than its free-ion value $gJ\mu_B = 7\mu_B$. This behavior is also seen in the Laves phases [46].

It can be concluded that since the ferrimagnetic configuration is energetically more stable than the FM one, there is an antiparallel coupling between the total magnetic moment of Gd that comes primarily from the localized 4f electrons and the transition-metal magnetic moments in all three amorphous cases. It is generally accepted that magnetism in crystalline intermetallic RE-TM compounds arises from the interaction between the RE 5d and TM 3d states [47,48]. The localized RE 4f electrons polarize the RE 5d states through local exchange interactions, and in turn the RE 5d and TM 3d states hybridize. The 5d and 3d moments are antiparallel [48] in Gd-TM systems, and consequently, crystalline $GdFe_2$ and $GdCo_2$ are ferrimagnets. In the amorphous cases one can observe the same behavior since this is a consequence of the sum rule of the magnetic moments in the d shell.

Another interesting observation is that in a-$GdNi_2$, Ni magnetic moments nearly disappear. This is not totally unexpected in RE-TM intermetallic compounds. Charge transfer

from the RE to the TM atoms can be anticipated due to the strong difference in electronegativity between the RE and TM atoms [49]. As a consequence, a large concentration of RE may contribute to fill the $3d$ band and therefore to reduce the splitting between the two $3d$ subbands (spin up and spin down). Finally, this leads to a reduction of the TM magnetic moment [50]. In fact, it has been a general consensus that Ni carries no magnetic moment in the intermetallic Laves compounds $RENi_2$ [51–53]. There have been recent reports, however, of small values for Ni magnetic moment, $\sim 0.2\mu_B$ in $GdNi_2$ [59].

$GdFe_2$ and $GdCo_2$ are, on the other hand, ferrimagnets in the Laves phases, where Fe and Co have magnetic moments of $\sim 2.1\mu_B$ [54,55] and $\sim 1.0\mu_B$ [50,57], respectively. For amorphous alloys the situation is similar. The measured values of the magnetic moments of Gd and Fe ions in amorphous films $Gd_{33}Fe_{67}$ are $7.22\mu_B$ and $2.01\mu_B$ [54], respectively. The calculated magnetic moment of Fe became higher than experiments. The LMTO-ASA study in Ref. [36] obtained magnetic moments of $7.2\mu_B$ for Gd and $-2.0\mu_B$ for Fe by placing the strongly localized Gd $4f$ electrons in the valence.

The total magnetic moment has been measured in Gd-Co amorphous ribbons, and for $Gd_{33}Co_{67}$ the magnetic moment of Co was $\sim 1.3\mu_B$ assuming that the magnetic moment of Gd was $7.0\mu_B$ [55]. This value is higher than the one in the crystalline Laves phase. Interestingly if one assumes that the magnetic moment of the Gd ions is a little higher, as the calculations in this study show, then the magnetic moment for Co ions would be $1.45\mu_B$, which is in very good agreement with the calculated value in this work. To my knowledge there is only one measurement for the total magnetic moment in a-$GdNi_2$ [56], $8.7\mu_B$, and the authors offered no explanation for this somehow unexpectedly high value. One could speculate that Ni and Gd magnetic moments couple ferromagnetically and that Ni has a high magnetic moment $\sim 0.8\mu_B$; however, from the calculations presented here and the experimental values in crystalline $GdNi_2$, this scenario appears unlikely.

Table III presents a summary of the magnetic moments for the $GdTM_2$ systems in amorphous and crystalline phases. In general, one can see that the magnetic moments do not change much between the amorphous and crystalline structures. The results for the Gd magnetic moments in the present calculation agree very well with experiments, and the values for Fe and Co are higher than experiments for $U = 3.0$ eV, while $U = 0.0$ eV gives reasonable magnetic moments. The possibility of noncollinear magnetism has not been explored in the present investigation. However, a small tilt on the moments could possibly reduce the magnetic moments on the TM sites. A more detailed study of the magnetic structure and exchange constants is ongoing and will be presented elsewhere.

TABLE III. Magnetic properties of amorphous and crystalline $GdTM_2$ alloys. Only the results for the ferrimagnetic configuration (see text) are listed for the three amorphous SQ structures for $U = 0$ (3) eV.

System	μ_{tot} (units of μ_B)	μ_{Gd} (units of μ_B)	μ_{TM} (units of μ_B)
$GdFe_2$ (SQ)	2.31 (1.9)	7.33 (7.5)	–2.51 (−2.8)
$GdFe_2$ (DRPH model)[a]	3.2	7.2	–2.0
a-$Gd_{33}Fe_{67}$[b]	3.3[c]	7.0	–1.85
a-$Gd_{33}Fe_{67}$[d]	3.2	7.22	–2.01
c-$GdFe_2$[d]	3.36	7.6	–2.12
$GdCo_2$ (SQ)	4.36 (3.8)	7.3 (7.24)	–1.47 (−1.7)
a-$Gd_{33}Co_{67}$[b]	4.4	7.0	–1.3[c]
a-$GdCo_2$[e]	4.2	7.0	–1.4[c]
c-$GdCo_2$[f]	4.8	7.0	–1.1[c]
$GdNi_2$ (SQ)	6.81 (6.62)	7.12 (7.12)	–0.17 (−0.25)
a-$GdNi_2$[e]	8.7		
c-$GdNi_2$[f]	7.1	7.0	–0.05[c]
c-$GdNi_2$[g]	6.52	7.0	–0.24[c]

[a]Experiments taken from Ref. [36].
[b]Experiments taken from Ref. [50] (amorphous film).
[c]The TM magnetic moment was obtained from the saturation magnetic moment at 4.2 K by assuming that the magnetic moment of Gd is $7\mu_B$.
[d]Experiments taken from Ref. [54] (amorphous films and crystal).
[e]Experiments taken from Ref. [56] (amorphous films).
[f]Experiments taken from Refs. [57,58] (crystal).
[g]Experiments taken from Ref. [59].

VI. CONCLUSIONS

The unique properties of BMGs are, to a large extent, due to their amorphous structure. Therefore, the study of the amorphous structure in glassy systems is very important for further developments of these materials. However, the absence of a crystal lattice complicates the analysis of experimental data, and therefore, the determination of the amorphous structure can be difficult and at times very challenging. In this study I used the SQ method to investigate structural and magnetic properties of BMG $GdTM_2$ (TM = Fe, Co, and Ni). This is a first-principles-based technique that has been shown to be very effective to find amorphous structures. In this work it was demonstrated that the SQ method can successfully be used to describe complex magnetic amorphous systems. In particular, it was shown that the amorphous structure is not strongly dependent on the magnetic configuration, and the atomic positions can be relaxed independently of the spin system. Interatomic distances and coordination numbers were calculated and were found to be in good agreement with experiments. Radial and angle distribution functions were also considered. From the structural analysis it can be concluded that the amorphous structures obtained by first-principles calculations are reliable models of these glassy systems. The SQ calculations demonstrated that the magnetic structure is ferrimagnetic for a-$GdFe_2$ and a-$GdCo_2$ and the magnetic moments of Fe and Co are smaller than those found in pure metallic Fe and Co, respectively. a-$GdNi_2$ is ferrimagnetic with a small contribution to the total magnetic moment from the Ni moments $\sim -0.17\mu_B$. The total calculated magnetic moments for a-$GdFe_2$, a-$GdCo_2$, and a-$GdNi_2$ are $2.31\mu_B$, $4.36\mu_B$, and $6.81\mu_B$, which are in good agreement with experiments.

ACKNOWLEDGMENTS

The author acknowledges support from the Chilean national agency Fondecyt Project Number 1120334 and also the supercomputer Ainil at the Instituto de Física y Matemáticas at

Universidad Austral de Chile. This work was supported also by the Swedish Research Council. Calculations were performed on resorces provided by the Swedish National Infrastructure for Computing (SNIC) at Linköping University in Sweden.

[1] *Bulk Metallic Glasses*, edited by M. Miller and P. Liaw (Springer, New York, 2008).
[2] *Rare Earths: New Reaserch*, edited by Z. Liu (Nova Science Publishers, New York, 2013), Chap. 8.
[3] J. Du, Q. Zheng, Y. B. Li, Q. Zhang, D. Li, and Z. D. Zhang, J. Appl. Phys. **103**, 023918 (2008).
[4] Q. Luo and W. H. Wang, J. Alloys Compd. **495**, 209 (2010).
[5] Q. Luo, D. Q. Zhao, M. X. Pan, and W. H. Wang, Appl. Phys. Lett. **89**, 081914 (2006).
[6] F. X. Qin, N. S. Bingham, H. Wang, H. X. Peng, J. F. Sun, V. Franco, S. C. Yu, H. Srikanth, and M. H. Phan, Acta Mater. **61**, 1284 (2013).
[7] N. S. Bingham, H. Wang, F. Qin, H. X. Peng, J. F. Sun, V. Franco, H. Srikanth, and M. H. Phan, Appl. Phys. Lett. **101**, 102407 (2012).
[8] B. Chevalier, J.-L. Bobet, J. S. Marcos, J. R. Fernandez, and J. G. Sal, Appl. Phys. A **80**, 601 (2005).
[9] D. A. Shishkin, A. S. Volegov, S. V. Adreev, and N. V. Baranov, Phys. Met. Metallogr. **113**, 460 (2012).
[10] H. Maeda, M. Sato, and M. Uehara, J. Jpn. Inst. Met. **47**, 688 (1983).
[11] C. Wu, D. Ding, L. Xia, and K. Chan, AIP Adv. **6**, 035302 (2016).
[12] T. D. Shen, R. B. Schwarz, J. Y. Coulter, and J. D. Thompson, J. Appl. Phys. **91**, 5240 (2002).
[13] V. Provenzano, A. J. Shapiro, and R. D. Shull, Nature (London) **429**, 853 (2004).
[14] X. Y. Liu, J. Barclay, R. B. Gopal, M. Földeáki, R. Chahine, T. K. Bose, P. J. Schurer, and J. L. LaCombe, J. Appl. Phys. **79**, 1630 (1996).
[15] P. Hohenberg and W. Kohn, Phys. Rev. **136**, B864 (1964).
[16] W. Kohn and L. Sham, Phys. Rev. **140**, A1133 (1965).
[17] E. Holmström, N. Bock, T. B. Peery, R. Lizárraga, G. De Lorenzi-Venneri, E. D. Chisolm, and D. C. Wallace, Phys. Rev. E **80**, 051111 (2009).
[18] E. Holmström, N. Bock, T. Peery, E. Chisolm, R. Lizárraga, G. De Lorenzi-Venneri, and D. Wallace, Phys. Rev. B **82**, 024203 (2010).
[19] R. Lizárraga, E. Holmström, A. Amézaga, N. Bock, T. Peery, E. Menendez-Proupin, and P. Giannozzi, J. Mater. Sci. **45**, 5071 (2010).
[20] R. Lizárraga, E. Holmström, S. C. Parker, and C. Arrouvel, Phys. Rev. B **83**, 094201 (2011).
[21] M. Saito, Y. Waseda, E. Matsubara, X.-M. Wang, T. Aihara, K. Aoki, and T. Masumoto, J. Non-Cryst. Solids **205–207**, 721 (1996).
[22] G. S. Cargill, III, in *Magnetism and Magnetic Materials—1973: Nineteenth Annual Conference*, AIP Conf. Proc. No. 18 (AIP, New York, 1974), p. 631.
[23] C. N. J. Wagner, N. Heiman, T. C. Huang, A. Onton, and W. Parrish, in *Magnetism and Magnetic Materials—1975*, AIP Conf. Proc. No. **29** (AIP, New York, 1976), p. 188.
[24] M. Matsuura, T. Fukunaga, K. Fukamichi, Y. Sato, and K. Suzuki, Z. Phys. Chem. **157**, 85 (1988).
[25] V. Petrov, K. Yano, and E. Kita, Phys. Status Solidi A **157**, 365 (1996).
[26] K. H. J. Buschow and A. M. van der Kraan, J. Magn. Magn. Mater. **22**, 220 (1981).
[27] K. H. J. Buschow, J. Less-Common Met. **79**, 9 (1981).
[28] K. H. J. Buschow, J. Less-Common Met. **66**, 89 (1979).
[29] K. H. J. Buschow, J. Magn. Magn. Mater. **21**, 97 (1980).
[30] K. H. J. Buschow, J. Appl. Phys. **51**, 2795 (1980).
[31] X. Yang, S. Ishio, and T. Miyazaki, IEEE Transl. J. Magn. Jpn. **5**, 431 (1990).
[32] K. Fukamichi, T. Goto, T. Sakakibara, S. Todo, K. Aoki, and T. Masumoto, J. Magn. Magn. Mater. **54–57**, 239 (1986).
[33] E. Kita, Y. Hata, K. Yano, K. Suzuki, and G. Kido, J. Appl. Phys. **95**, 6834 (2004).
[34] C. L. Zhang, D. H. Wang, Z. D. Han, H. C. Xuan, B. X. Gu, and Y. W. Du, J. Appl. Phys. **105**, 013912 (2009).
[35] X. Zhong, P. Tang, Z. Liu, D. Zeng, Z. Zheng, H. Yu, W. Qiu, and M. Zou, J. Alloys Compd. **509**, 6889 (2011).
[36] H. Tanaka, S. Takayama, and T. Fujiwara, Phys. Rev. B **46**, 7390 (1992).
[37] R. Chimata, L. Isaeva, K. Kádas, A. Bergman, B. Sanyal, J. H. Mentink, M. I. Katsnelson, T. Rasing, A. Kirilyuk, A. Kimel *et al.*, Phys. Rev. B **92**, 094411 (2015).
[38] D. C. Wallace, *Statistical Physics of Crystals and Liquids* (World Scientific, Singapore, 2002).
[39] VASP is a package for performing *ab initio* quantum-mechanical molecular dynamics using pseudopotentials and a plane-wave basis set; http://cms.mpi.univie.ac.at/vasp/.
[40] G. Kresse and J. Furthmüller, Phys. Rev. B **54**, 11169 (1996).
[41] S. L. Dudarev, G. A. Botton, S. Y. Savrasov, C. J. Humprheys, and A. P. Suttom, Phys. Rev. B **57**, 1505 (1998).
[42] P. E. Blöchl, Phys. Rev. B **50**, 17953 (1994).
[43] J. M. D. Coey, *Magnetism and Magnetic Materials* (Cambridge University Press, Cambridge, 2010).
[44] A. H. Narten and H. A. Levy, Science **165**, 447 (1969).
[45] J. H. Wernick, *Intermetallic Compounds* (Wiley, New York, 1967).
[46] N. V. Mushnikov, T. Goto, V. S. Gaviko, and N. K. Zajkov, J. Alloys Compd. **292**, 51 (1999).
[47] I. A. Campbell, J. Phys. F **2**, L47 (1972).
[48] M. S. S. Brooks, L. Nordström, and B. Johansson, J. Phys.: Condens. Matter **3**, 2357 (1991).
[49] A. R. Miedema, R. Boom, and F. R. de Boer, J. Less-Common Met. **41**, 283 (1973).
[50] K. H. J. Buschow, M. Brouha, J. W. M. Biesterbos, and A. G. Dirks, Physica B+C **91**, 261 (1977).
[51] G. Chelkowska and M. Neumann, Solid State Commun. **91**, 799 (1994).
[52] E. Dormann and K. H. J. Buschow, Phys. B (Amsterdam, Neth.) **86–88**, 75 (1977).
[53] V. L. B. de Jesus, I. S. Oliveira, P. C. Riedi, and A. P. Guimaraes, J. Magn. Magn. Mater. **212**, 125 (2000).

[54] C. Vittoria, P. Lubitz, and V. Ritz, J. Appl. Phys. **49**, 4908 (1978).
[55] K. H. J. Buschow and A. M. van Diepen, Solid State Commun **19**, 79 (1976).
[56] K. Lee and N. Heiman, in *Magnetism and Magnetic Materials—1974: 20th Annual Conference, San Francisco*, AIP Conf. Proc. No. 24 (AIP, New York, 1975), p. 108.
[57] R. Lemaire and J. Schweizer, Phys. Lett. **21**, 366 (1966).
[58] K. H. J. Buschow, Rep. Prog. Phys. **40**, 1179 (1977).
[59] K. Yano, I. Umehara, T. Miyazawa, Y. Adachi, and K. Sato, Phys. B (Amsterdam, Neth.) **367**, 81 (2005).